

Cardiac Energy Dependence on Glucose Increases Metabolites Related to Glutathione and Activates Metabolic Genes Controlled by Mechanistic Target of Rapamycin

Jonathan C. Schisler, PhD; Trisha J. Grevengoed, BS; Florencia Pascual, PhD; Daniel E. Cooper, BS; Jessica M. Ellis, PhD; David S. Paul, PhD; Monte S. Willis, MD, PhD; Cam Patterson, MD; Wei Jia, PhD; Rosalind A. Coleman, MD

Background—Long chain acyl-CoA synthetases (ACSL) catalyze long-chain fatty acids (FA) conversion to acyl-CoAs. Temporal ACSL1 inactivation in mouse hearts (*Acs11*^{H⁻/-}) impaired FA oxidation and dramatically increased glucose uptake, glucose oxidation, and mTOR activation, resulting in cardiac hypertrophy. We used unbiased metabolomics and gene expression analyses to elucidate the cardiac cellular response to increased glucose use in a genetic model of inactivated FA oxidation.

Methods and Results—Metabolomics analysis identified 60 metabolites altered in *Acs11*^{H⁻/-} hearts, including 6 related to glucose metabolism and 11 to cysteine and glutathione pathways. Concurrently, global cardiac transcriptional analysis revealed differential expression of 568 genes in *Acs11*^{H⁻/-} hearts, a subset of which we hypothesized were targets of mTOR; subsequently, we measured the transcriptional response of several genes after chronic mTOR inhibition via rapamycin treatment during the period in which cardiac hypertrophy develops. Hearts from *Acs11*^{H⁻/-} mice increased expression of several *Hif1* α -responsive glycolytic genes regulated by mTOR; additionally, expression of *Sc17a5*, *Gsta1/2*, *Gdf15*, and amino acid-responsive genes, *Fgf21*, *Asns*, *Trib3*, *Mthfd2*, were strikingly increased by mTOR activation.

Conclusions—The switch from FA to glucose use causes mTOR-dependent alterations in cardiac metabolism. We identified cardiac mTOR-regulated genes not previously identified in other cellular models, suggesting heart-specific mTOR signaling. Increased glucose use also changed glutathione-related pathways and compensation by mTOR. The hypertrophy, oxidative stress, and metabolic changes that occur within the heart when glucose supplants FA as a major energy source suggest that substrate switching to glucose is not entirely benign. (*J Am Heart Assoc.* 2015;4:e001136 doi: 10.1161/JAHA.114.001136)

Key Words: acyl-CoA synthetase • fuel switching • glutathione • mTOR • oxidative stress

In the heart, long-chain fatty acids (FA) of 14 to 20 carbons are the major substrates for energy production^{1,2} and provide 60% to 90% of the ATP used for

contraction.³ Cardiac hypertrophy resulting from systemic hypertension, ischemia, and infarction is associated with a metabolic switch in fuel substrates, decreasing FA oxidation while increasing glucose metabolism.⁴ Whereas some mouse models suggest that hypertrophy signaling pathways contribute to the switch to glucose metabolism and that increased glucose use alone is not sufficient to promote cardiac hypertrophy,^{5–7} a study of ex vivo working hearts showed that dependence on glucose precedes functional heart remodeling in response to hemodynamic stress,⁸ highlighting the intricacies between cardiac growth and metabolism.

We have developed a mouse model in which hypertrophy results from fuel switching from FA to glucose. A cardiomyocyte-specific deficiency of long-chain acyl-CoA synthetase-1 (*Acs11*) prevents the use of FA for oxidation. Thus, ACSL1-deficient hearts (*Acs11*^{H⁻/-}) depend on the oxidation of glucose, amino acids, and ketones for contractile energy⁹ and progressively develop cardiac hypertrophy.¹⁰

From the Division of Cardiology, Department of Medicine (J.C.S., C.P.), Department of Nutrition (T.J.G., F.P., D.E.C., J.M.E., D.S.P., R.A.C.), and Department of Pathology and Laboratory Medicine (M.S.W.), University of North Carolina, Chapel Hill, NC; Nutrition Research Institute, Kannapolis, NC (W.J.).

Dr Jia is currently located at the University of Hawaii Cancer Center, Honolulu, HI.

Dr Ellis is currently located at the Purdue University, West Lafayette, IN.

An accompanying Table S1 is available at <http://jaha.ahajournals.org/content/4/2/e001136/suppl/DC1>.

Correspondence to: Rosalind A. Coleman, MD, Michael Hooker Research Center, 135 Dauer Drive, Department of Nutrition, CB# 7461, University of North Carolina at Chapel Hill, Chapel Hill, NC 27599. E-mail: rcoleman@unc.edu
Received May 23, 2014; accepted January 28, 2015.

© 2015 The Authors. Published on behalf of the American Heart Association, Inc., by Wiley Blackwell. This is an open access article under the terms of the Creative Commons Attribution-NonCommercial License, which permits use, distribution and reproduction in any medium, provided the original work is properly cited and is not used for commercial purposes.

ACSL1, a membrane-associated enzyme present on the mitochondria and endoplasmic reticulum that catalyzes the activation of long-chain FA to form acyl-CoA, is 1 of 5 closely related long-chain acyl-CoA synthetase isoforms. ACSL1 is highly expressed in oxidative tissues like brown adipose tissue and heart, and depleting cardiac *Acs1* expression results in a 90% decrease in the mitochondrial oxidation of long-chain acyl-CoAs.⁹ In contrast, overexpression of ACSL1 in heart causes toxicity and cell death, probably due to a mismatch between the production of acyl-CoAs and their incorporation into downstream pathways.¹¹ Endogenous ACSL1 in heart directs its acyl-CoA product towards β -oxidation rather than towards the synthesis of complex lipids.⁹ Consistent with the switch to glucose metabolism in *Acs1*^{H^{-/-}} hearts, uptake of the FA analog 2-Br[¹⁴C]palmitate decreases 35%, while uptake of 2-deoxy[¹⁴C]glucose increases 8-fold.^{9,10} Although one might predict that *Acs1*^{H^{-/-}} hearts have low energy stores, the cardiac energy sensor AMP-activated kinase (AMPK) is not activated; instead, the mechanistic target of rapamycin (mTOR), a kinase that drives cardiac growth by promoting protein synthesis and enhancing glucose and lipid metabolism,¹² is robustly activated.⁹ mTORC1 is activated by signals of nutrient availability, including insulin and other growth factors, amino acids, and adequate energy levels (oxygen availability and low AMPK activity).¹³ The hypertrophy that occurs in *Acs1*^{H^{-/-}} hearts is primarily mTOR-dependent, as hypertrophy is blocked after treatment of *Acs1*^{H^{-/-}} mice with rapamycin.¹⁰ In order to understand the full extent of the metabolic pathways that change concomitantly with the forced substrate switch away from FA oxidation, we performed unbiased gene array and metabolomics analyses. We asked whether the expression of specific genes would be altered in a similar fashion to those previously identified as downstream targets of mTOR in mouse embryo fibroblasts (MEFs),¹⁴ because such changes might reveal previously unappreciated aspects of mTOR regulation of cardiac metabolism.

Methods

Animal Treatment

The University of North Carolina Institutional Animal Care and Use Committee approved the mouse protocols. Mice were housed in a pathogen-free barrier facility (12-hour light/dark cycle) with free access to water and food (Prolab RMH 3000 SP76 chow). Mice with *LoxP* sequences inserted on either side of exon 2 in the *Acs1* gene¹⁵ were backcrossed 6 times to C57Bl/6 mice and then interbred with mice in which Cre expression is driven by an α -myosin heavy chain promoter induced by tamoxifen (B6.Cg-Tg(Myh6-cre/Esr1)1Jmk/J, Jackson Labs) to generate tamoxifen-inducible, heart-specific

Acs1^{H^{-/-}} knockout mice.⁹ At 6 to 8 weeks of age, *Acs1*^{H^{-/-}} and littermate *Acs1*^{flox/flox} control male mice were injected i.p. with tamoxifen (75 mg/kg BW; Sigma), dissolved in corn oil (20 mg/mL) for 4 consecutive days (3 mg/40 g BW). Subgroups of mice were also injected daily i.p. for 10 weeks with rapamycin (1 mg/kg in PBS, 8% ethanol, 10% Tween 20, 10% PEG-400; Sigma) or with vehicle alone. Ten weeks after tamoxifen induction, animals were anesthetized with 2,2,2-tribromoethanol, and heart ventricles were removed and snap frozen in liquid nitrogen. Protein content was determined by the BCA assay (Pierce) with bovine serum albumin as the standard. Plasma was collected from mice in 5% 0.5 mol/L EDTA.

Immunoblots

Heart homogenates were prepared in isolation buffer (250 mmol/L sucrose, 10 mmol/L HEPES, 1 mmol/L EDTA, 1 mmol/L dithiothreitol, plus Halt Protease and Phosphatase Inhibitor Cocktail [1861280, Thermo Scientific]) and crude mitochondrial and cytosolic fractions were obtained by differential centrifugation. Total protein lysates were isolated in lysis buffer (250 mmol/L sucrose, 20 mmol/L Tris, 1% Triton X-100, 50 mmol/L NaF, 50 mmol/L NaCl, 5 mmol/L Na₄P₂O₇, plus Halt Protease and Phosphatase Inhibitor Cocktail). For GLUT1 Western blots, lysates were treated with PNGase F deglycosylation kit (P0704S; New England Biolabs) prior to SDS-PAGE.¹⁶ Tissue proteins were blotted with primary antibodies to detect GSK-3 β , P-p70 S6 kinase (Thr389), p70 S6 kinase, P-4E-BP1 (Thr37/46), 4E-BP1, ACSL1 (9315, 9234, 9202, 2855, 9644 and 4047, respectively; Cell Signaling Technology), VDAC1, PDK4, GLUT1, and GAPDH (ab15895, ab38242, ab40084, and ab8245, respectively; Abcam).

Pyruvate Oxidation

Oxidation of pyruvate was performed as previously described.⁹ Freshly isolated heart ventricles and livers were minced and homogenized with 10 up-and-down strokes using a motor-driven Teflon pestle and glass mortar in ice-cold buffer (250 mmol/L sucrose, 1 mmol/L EDTA, 10 mmol/L HEPES, pH 7.4) at a 20-fold dilution (wt/vol). Homogenates were centrifuged at 500g for 5 minutes. Oxidation was measured in a 200 μ L reaction mixture containing 100 mmol/L sucrose, 10 mmol/L Tris-HCl, 10 mmol/L KPO₄, 100 mmol/L KCl, 1 mmol/L MgCl₂·6H₂O, 1 mmol/L L-carnitine, 0.1 mmol/L malate, 2 mmol/L ATP, 0.05 mmol/L coenzyme A, and 1 mmol/L dithiothreitol (pH7.4) with 5 mmol/L pyruvate (0.2 μ Ci of [1-¹⁴C]pyruvate for PDH activity or [2-¹⁴C]pyruvate for TCA cycle flux). Oxidation studies measured the production of ¹⁴C-labeled carbon

dioxide (CO₂) for 30 minutes without substrate competition in a 2-well oxidation system, the assay well containing the reaction mixture with the tissue homogenate, and the adjoining well containing 1 N NaOH. The reaction was terminated by adding 70% perchloric acid to the assay well and the plate was incubated for 1 hour to drive the CO₂ into the NaOH. Radioactivity of CO₂ was determined by liquid scintillation counting.

Oxidative Stress

For glutathione measurements, tissues were homogenized in 5% 5-sulfo-salicylic acid dehydrate to remove protein. Samples were treated with 2-vinylpyridine to block free GSH and other thiols present. GSH/GSSG was measured using a colorimetric kit (K006-H1; Arbor Assays). For measures of DNA and RNA damage, 8-hydroxy-2'-deoxyguanosine and 8-hydroxyguanosine were measured in 250 to 500 ng total nucleic acids extracted from left ventricles using an enzyme immunoassay (589320; Cayman Chemical).

Gene Expression Analysis

Total RNA was isolated from heart ventricles (RNeasy Fibrous Tissues Kit; Qiagen). RNA integrity was verified on an Agilent BioAnalyzer 2100 (RIN \geq 9). For microarray analysis, cyanine-5-labeled cRNA was co-hybridized to the G4122F mouse whole genome array (Agilent) with equimolar amounts of cyanine-3-labeled mouse reference RNA¹⁷ and scanned on a GenePix 4000B (Axon) with Feature Extraction (v9.5.3.1; Agilent). In at least 3 of the 4 biological replicates per condition, 9633 probes were present, and these were used for principal component analysis (PCA), resulting in the identification of a single wild-type outlier (data not shown). To determine differentially expressed genes between genotypes, a gene-level analysis was performed (GeneSpring GX, v12.4) that incorporated multiple probes (Lowess normalization) into a single gene value. Genes that were not detected in at least 2 of the biological replicates per genotype were filtered and removed, resulting in 7610 genes. The gene values were used for PCA, hierarchical clustering, and significance of microarray analysis (SAM).¹⁸ Functional enrichment on gene clusters determined the fold enrichment using the Database for Annotation, Visualization and Integrated Discovery (DAVID).¹⁹ For qPCR analysis, cDNA was synthesized (High Capacity cDNA RT Kit; Applied Biosystems) and 10 ng of cDNA was added to each qPCR reaction with SYBR Green (Applied Biosystems) and used to detect amplicons with primers specific to the gene of interest (Table 1) quantified using a qPCR thermocycler (BioRad). Results were normalized to the housekeeping gene *Gapdh* and expressed as arbitrary units of $2^{-\Delta\Delta CT}$ relative to the control group.

Tissue Sample Preparation and Analysis by Gas Chromatography-Time of Flight Mass Spectrometry (GC-TOFMS)

Tissue sample preparation and analysis by GC-TOFMS was performed as described.^{20,21} Approximately 50 mg of each tissue sample was prepared using a 2-step extraction. The tissue sample was first added with 50 μ L of the first-step extraction solvent (chloroform:methanol:water; 1:2.5:1) and homogenized for 6 minutes in a bullet blender (BIOBOXTM; Next Advance, Inc). The sample was extracted with another 250 μ L of the first-step extraction solvent, and centrifuged at 16 750 \times g for 20 minutes at 4°C. A 100 μ L aliquot of the supernatant was transferred to a GC sampling vial. At the second step, the deposit of tissue was extracted with 300 μ L methanol. After centrifuging at 13 200 rpm for 20 minutes at 4°C, a 100 μ L aliquot of supernatant was transferred to the same GC vial. After vortexing, the samples were spiked with 2 internal standards (10 μ L heptadecanoic acid at 1 mg/mL and 4-chlorophenylalanine at 0.3 mg/mL) and were vacuum dried at room temperature. The residue was derivatized using a 2-step procedure. First, 80 μ L methoxyamine (15 mg/mL in pyridine) was added to the vial and kept at 30°C for 90 minutes. Then, 80 μ L BSTFA (1% TMCS) was added to the samples, before being derivatized at 70°C for 60 minutes.

Each 1 μ L aliquot of the derivatized solution was injected in splitless mode into an Agilent 6890N gas chromatography coupled with a Pegasus HT time-of-flight mass spectrometry (GC-TOFMS) (Leco Co). To minimize systematic analytical deviations, samples from 2 groups were run in alternating order. Separation was achieved on an Rxi-5ms capillary column (Crossbond 5% diphenyl/95% dimethyl polysiloxane, Restek), with helium as the carrier gas at a constant flow rate of 1.0 mL/min. The temperatures of injection, transfer interface, and ion source were set to 260, 260, and 210°C, respectively. The GC temperature programming was set to 2 minutes isothermal heating at 80°C, followed by 10°C/min oven temperature ramped to 220°C, 5°C/min to 240°C, and 25°C/min to 290°C, and a final 8 minutes maintenance at 290°C. Electron impact ionization (70 eV) at full scan mode (m/z 40 to 600) was used, with an acquisition rate of 20 spectra/sec in the TOFMS setting.

The data generated in the GC-TOFMS instrument were analyzed by the ChromaTOF software (v4.33; Leco Co). Compound identification was performed by comparing the mass fragments with NIST 05 Standard mass spectral databases in NIST MS search 2.0 (NIST) software with a similarity of more than 70% and reference standards. Internal standards and known artificial peaks caused by noise, column bleed, or the BSTFA derivatization procedure were removed from the dataset before statistical analysis.

Table 1. DNA Oligonucleotide Primer Sequences Used for qPCR Analysis of mRNA Expression in Mouse Heart

cDNA	Forward Primer	Reverse Primer
<i>Acot1</i>	GGAGGGGAGCCCAAGCCTCA	TTCCAGCCCTTGAATCAGCAC
<i>Acot2</i>	GCGCGGCTGTTGTACCTCC	CATCGGGCTCGTGTCCGTCC
<i>Asns</i>	GCGGCCTCCAACCGGTCTTGTC	GCTACAGGCGGACTGCAGGCA
<i>Chrebp</i>	CTGCTCAGGGCAGCCAAGCC	CCAGGGACCTGGGAGGAGCC
<i>Gapdh</i>	GGTGTGAGTATGTCTGGA	ACTGTGGTCATGAGCCCTTC
<i>Gdf15</i>	GCTATGCTGCCCTCTGGCGG	TCGCCCCACGCATGCTCAG
<i>Gpr22</i>	AGATCGTGTGGGGCTGGCA	CTGCCGTTCTCGTGTCCCG
<i>Gsta1</i>	CCGTGCTTCACTACTTCAAT	GCATCCATGGGAGGCTTCT
<i>Hif1a</i>	TCAAGTCGTGAATAATACC	CCACAGGACAGTACAGGATG
<i>Mthfd2</i>	CAGTGCGAAATGAAGCCGTT	GCTGCCCTGGTTTTGTTGAG
<i>Myc</i>	GTTGGAACCCCGCAGACAG	ATAGGGCTGTACGGAGTCGT
<i>Pdk4</i>	CCGCTGTCCATGAAGCA	GCAGAAAAGCAAAGGACGTT
<i>Pfkfb1</i>	CCACCGGACCTGCTTTGGGG	GGCCTCCATGTTGTCTGGGCG
<i>Sesn1</i>	CCGCTGACCCTGCGACACAGA	TTCCCCAAAGCAGCCCGTC
<i>Slc7a5</i>	AGTGCCTCAAGGGGACCGCA	GACTTCAGGGCGGGCAGAGC
<i>Srebp1</i>	GTAGGTCACCGTTTCTTTGTGGAC	TGGGCTGAGCAATACAGTTCAAC
<i>Trib3</i>	GCGACCTCAAGCTGCGTCGC	TGGTCCCACGTAGGCAGGGCA
<i>Trib3</i>	GCGACCTCAAGCTGCGTCGC	TGGTCCCACGTAGGCAGGGCA

Sequences are listed in the 5' to 3' orientation.

Tissue Sample Preparation and Analysis by Liquid Chromatography-Time of Flight Mass Spectrometry (LC-TOFMS)

Tissue sample preparation and analysis with LC-TOFMS were performed as described.^{21–23} Tissue samples (50 mg) were homogenized on ice in 500 μ L of chloroform/methanol/water (1:2.5:1, v/v/v). Samples were then centrifuged at 16 250 \times g for 10 minutes at 4°C, and a 150 μ L aliquot of the supernatant was transferred to an LC sampling vial containing an internal standard (10 μ L L-4-chloro-phenylalanine in water, 5 μ g/mL). The deposit was re-homogenized with 500 μ L of methanol, and a 150 μ L aliquot of supernatant was added to the same vial. The extract was centrifuged at 13 000 rpm for 20 minutes, and the supernatant was used for LC-TOFMS analysis.

An Agilent HPLC 1200 system equipped with a binary solvent delivery manager and a sample manager (Agilent Corporation) was used with chromatographic separations performed on a 4.6 \times 150 mm 5 μ m Agilent ZORBAX Eclipse XDB-C18 chromatography column. The LC elution conditions were optimized as follows: isocratic at 1% B (0 to 0.5 minutes), linear gradient from 1% to 20% B (0.5 to 9.0 minutes), 20% to 75% B (9.0 to 15.0 minutes), 75% to 100% B (15.0 to 18.0 minutes), isocratic at 100% B (18.0–19.5 minutes); linear gradient from 100% to 1% B (19.5 to 20.0 minutes)

and isocratic at 1% B (20.0–25.0 minutes). Here, A=water with 0.1% formic acid and B=acetonitrile with 0.1% formic acid. The column was maintained at 30°C. A 10 μ L aliquot sample was injected onto the column. Mass spectrometry was performed using an Agilent model 6220 MSD TOF-MS equipped with a dual sprayer electrospray ionization source (Agilent Corporation). The system was tuned for optimum sensitivity and resolution using an Agilent ESI-L low concentration tuning mix in both positive (ES+) and negative (ES–) electrospray ionization modes. An Agilent API-TOF reference mass solution kit was used to obtain accurate mass TOF data in both positive and negative modes. The TOF MS was operated under the following optimized conditions: (1) ES+ mode, capillary voltage 3500 V, nebulizer 45 psig, drying gas temperature 325°C, drying gas flow 11 L/min, and (2) ES– mode, similar conditions as ES+ mode except the capillary voltage that was adjusted to 3000 V. The TOF-MS is calibrated routinely in ES+ and ES– modes using the Agilent ESI-L low concentration tuning mix. During metabolite profiling experiments, both plot and centroid data were acquired for each sample from 50 to 1000 Da over a 25-minute analysis time.

The resulting .d files were then centroided, deisotoped, and converted to mzData xml files using the MassHunter Qualitative Analysis Program (vB.03.01) (Agilent). After the conversion, the xml files were analyzed using the open source

XCMS package (v1.24.1) (<http://metlin.scripps.edu>), which runs in the statistical package R (v.2.12.1) (<http://www.r-project.org>), to pick, align, and quantify features (chromatographic events corresponding to specific m/z values and retention times). The created .tsv file was opened using Excel software and saved as an .xls file. The resulting data sheet was used for further multivariate and univariate statistical analysis. Metabolite annotation was performed by comparing the accurate mass (m/z) and retention time (Rt) of reference standards in our in-house library and the accurate mass of compounds obtained from the web-based resources such as the Human Metabolome Database (<http://www.hmdb.ca/>).

Metabolomic Analysis

Metabolite concentrations were analyzed using Metaboanalyst (v2.0)^{24–26} run in the statistical package R (v2.14.0). Concentrations were log transformed and mean-centered resulting in a Gaussian distribution of metabolite concentrations. The normalized data was used for PCA and partial least squares discriminant analysis (PLS-DA). A moderated t-statistic model (SAM)¹⁸ was used to identify metabolites that were different between genotypes at a false discovery rate less than 5% and clustered using Euclidean dissimilarity and average linkage (Partek Genomics Suite, v6.6).

Statistics

Values are expressed as mean±standard error of the mean (SEM) as indicated. Statistical analysis of qPCR data comparing *Acs1*^{H^{-/-}} and *Acs1*^{flox/flox} for array validation was performed using a 1-tailed unpaired *t* test. For studies that included rapamycin treatments, 2-way ANOVA was used with the genotype and treatment identified as the sources of variation. Post-hoc tests were performed with Tukey's multiple comparisons test. For all tests, *P*>0.05 was considered non-significant (ns).

Results

Genomic Analysis Identified Novel Gene Expression Patterns in *Acs1*^{H^{-/-}} Ventricles

Acs1^{H^{-/-}} mice have impaired cardiac FA oxidation and develop spontaneous cardiac hypertrophy due to increased mTOR activation.¹⁰ To explore how the loss of ACSL1 alters mRNA regulation, we performed a global gene expression analysis on ventricular RNA isolated from *Acs1*^{H^{-/-}} and *Acs1*^{flox/flox} mice 10 weeks after tamoxifen treatment, when ACSL1 protein is completely absent and the ACSL-specific activity in *Acs1*^{H^{-/-}} hearts is reduced 90%.⁹ PCA identified the genotype as a primary variable contributing to the

differences in global gene expression (Figure 1A, principal component 1, 33% of the total variance), which was further confirmed via unsupervised hierarchical clustering (Figure 2A). Significance analysis of microarrays (SAM) identified 568 differentially expressed genes at a false discovery rate less than 4.36% (Figures 1B and 2B, Table S1).

In MEFs with increased mTOR activity, the transcription factors *Srebf1* and *Hif1α* mediate downstream mTORC1 pathways, including lipid biosynthesis, the pentose phosphate shunt, and glycolysis.¹⁴ Activation of mTOR in *Acs1*^{H^{-/-}} hearts was shown in previous studies¹⁰ as well as in the current work by a 6-fold increase in phosphorylated S6 kinase (S6K); additionally, variations in the amount of phosphorylation led to a non-significant 3-fold increase in phosphorylation of 4E-BP1, a second mTOR target examined (Figure 3A). Given both the activation of mTOR and the cardiac hypertrophy that develops in *Acs1*^{H^{-/-}} hearts,⁹ we hypothesized that changes related to mTORC1 and hypertrophy would be reflected at the mRNA level. In fact, the expression of both *Srebf1* and *Hif1α* was increased, as well as their respective targets *Trib3*²⁷ and *Pdk4*,^{28,29} which regulate glucose metabolism (Table 2, Table S1, Figure 3B and 3C). These changes coincide with an 8-fold higher uptake of 2-deoxy[¹⁴C]glucose by *Acs1*^{H^{-/-}} hearts compared with controls.¹⁰ Consistent with the cardiac hypertrophy, the hypertrophy-associated gene *Myc* increased

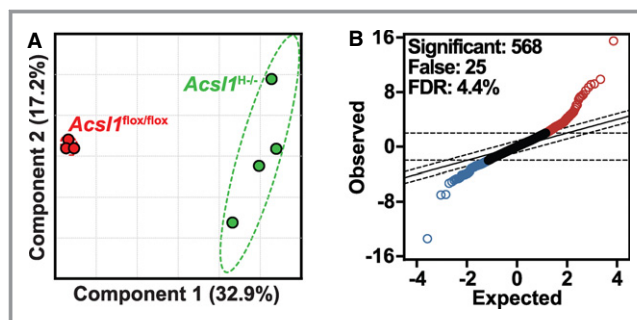


Figure 1. Global changes in gene expression in *Acs1*^{H^{-/-}} hearts. A, Principal component analysis (PCA) of global changes in cardiac gene expression was performed using the levels of 7581 genes in *Acs1*^{flox/flox} (red closed circles) and *Acs1*^{H^{-/-}} (green closed circles) mice after 10 weeks of rapamycin treatment, represented by a scatter plot of the first (PC1) vs second principal component (PC2). Four eigenvectors were calculated for PCA and data represented in the scatter plot are scaled to unit standard deviation. Confidence ellipses categorized by genotype represent 2 standard deviations. B, Significance analysis of microarrays (SAM) plot of observed scores plotted against the expected scores. The solid line represents observed=expected, whereas the hashed lines indicate the significance threshold based on $\Delta=0.851$. The genes identified as differentially expressed are indicated by red and blue open circles, indicating higher and lower expression, respectively, of these genes in *Acs1*^{H^{-/-}} mouse hearts. The number of differentially expressed genes, predicted false positives, and the false discovery rate (FDR) are provided (also see Figure 2A and 2B).

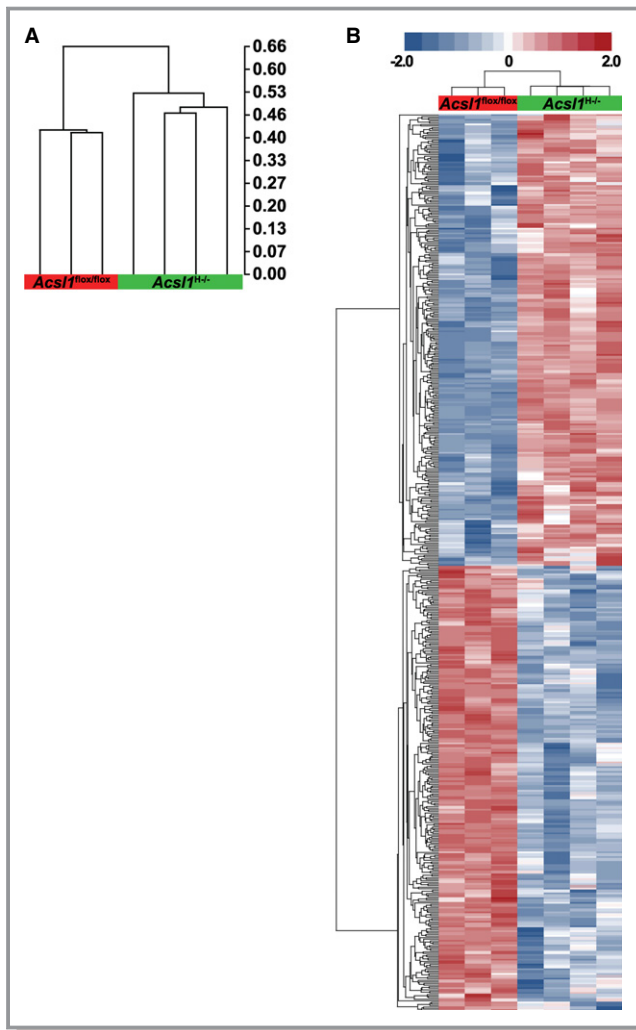


Figure 2. Unsupervised gene clustering. A, Unsupervised hierarchical clustering was used to reveal natural categories in gene expression data sets. Expression values from the 7162 genes detected via microarray analysis were analyzed by sample clustering using Pearson's Dissimilarity matrix with average linkage (Partek Genomics Suite, v6.6). Two primary clusters of microarray samples were comprised solely of either *Acs1*^{flox/flox} (red) or *Acs1*^{H-/-} (green) biological replicates. The scale for the dendrogram represents the distance of clusters by Pearson's correlation coefficient. B, Unsupervised clustering of the 568 SAM positive genes. The expression values from the 568 genes (rows) from 7 samples (columns) detected as differentially expressed via microarray analysis were analyzed with hierarchical clustering using the Euclidian matrix with average linkage (Partek Genomics Suite, v6.6). As expected based on the 2 class SAM analysis used to identify differentially expressed genes, we identified 2 primary clusters of microarray samples comprised solely of either *Acs1*^{flox/flox} (red) or *Acs1*^{H-/-} (green) biological replicates. Additionally, the genes portioned into 2 groups of higher (maroon) or lower (blue) expression across the 2 genotypes. SAM indicates significance analysis of microarrays.

5- to 6-fold (Table 2, Figure 3B). Growth differentiation factor 15 (*Gdf15*), one of the most highly up-regulated genes observed (Table 2, Table S1, Figure 3B), is upregulated by

events that cause oxidative stress in heart and is considered to be protective against apoptosis and fibrosis.³⁰

Other pathways that were altered by the temporal loss of cardiac *Acs1* expression included functional clusters that correlated with differential gene expression (Table 3). The clusters that increased in *Acs1*^{H-/-} hearts primarily involved cellular metabolism (amino acids (eg, *Slc7a5*; large neutral amino acid transporter small subunit-1), lipids, flavoproteins, and several peroxisomal genes), protein synthesis (aminoacyl-tRNA synthetases and ribosomal genes), and additional genes involved in cardiac remodeling, such as *MuRF1* (*Trim63*), *Abra*, and *Cryab*. Also increased in *Acs1*^{H-/-} hearts was the expression of the tRNA synthetase *Lars*, as well as several other tRNA-synthetases (*Cars*, *Nars*, *Sars*, and *Aars*), consistent with the increases in mTORC1 activity and protein synthesis. LARS activates mTOR through its non-canonical role as a GTPase-activating protein for Rag GTPase that directly activates mTORC1, thereby linking amino acid metabolism and mTOR activation.

Down-regulated genes in *Acs1*^{H-/-} hearts relative to control hearts were primarily genes involved in transcriptional regulation, such as *Pparα*, as well as 22 zinc finger genes (Table 3). Additional functional categories that were down-regulated included apoptotic regulatory genes and genes involved in striated muscle development, consistent with the extensive remodeling observed in *Acs1*^{H-/-} hearts.

Enhanced Amino Acid Response and Glutathione S-Transferase Gene Expression in *Acs1*^{H-/-} Hearts

The shift from FA to glucose as the heart's primary fuel substrate has been observed in many models of cardiac pathology and injury. Whether the substrate switch is adaptive or maladaptive remains an ongoing debate.^{31,32} Nevertheless, because the heart is metabolically resilient, we hypothesized that the *Acs1*^{H-/-} mouse model would reveal additional metabolic pathways not appreciated in previous studies of hypertrophy or substrate switching. The most up-regulated genes in *Acs1*^{H-/-} hearts (range=4- to 38-fold, q-value=0.00; Table S1) were involved in either the amino acid response³³ (*Fgf21*, *Gdf15*, *Mthfd2*, *Trib3*, *Asns*) or glutathione metabolism (*Gsta1*) (Table 2, Figure 3B). Several human and rodent models of skeletal muscle mitochondrial myopathy, including mitochondrial encephalomyopathy, lactic acidosis, and stroke-like episodes (MELAS syndrome), progressive external ophthalmoplegia, and the deletor mouse, also show a similar response with upregulation of the same genes.³⁴⁻³⁶ The promoter regions of the amino acid responsive genes contain consensus sequences for the conserved amino acid response element (AARE); thus, because both *Asns* and *Mthfd2* are involved in amino acid synthesis, it is likely that an increased

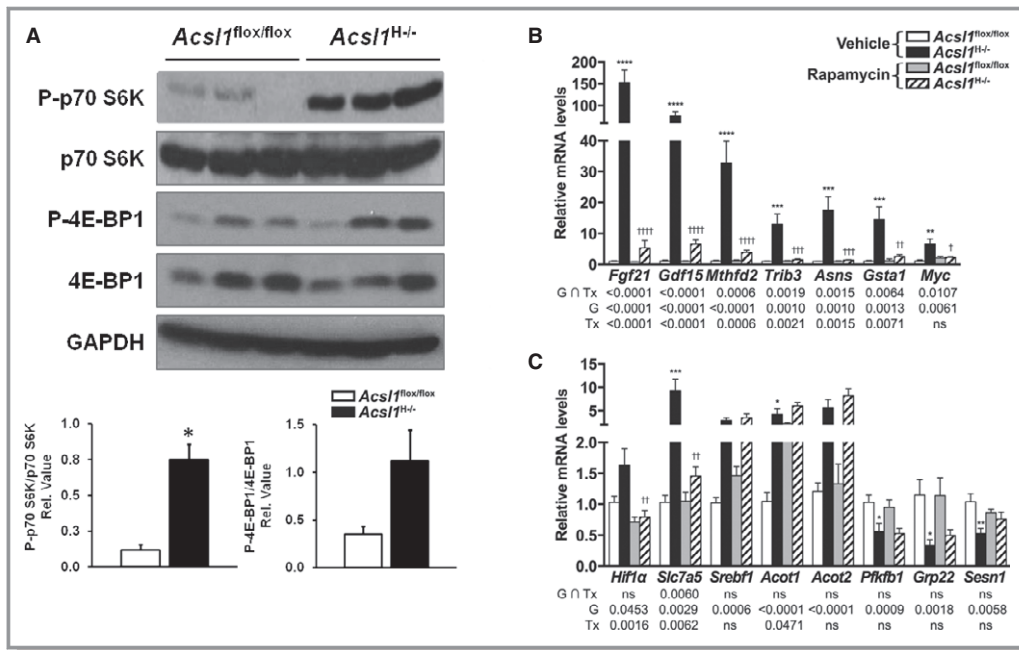


Figure 3. mTOR activation and expression of selected genes in ventricles from control and *Acs1*^{H-/-} mice treated with vehicle or rapamycin for 10 weeks. A, Representative immunoblots from ventricles of male mice 10 weeks after tamoxifen treatment. The levels of total and phosphorylated (P-p70 S6K [Thr389], P-4E-BP1 [Thr37/46]) p70 S6K and 4E-BP1 were quantified with ImageJ software, and the ratio of phosphorylated to total protein is shown (bottom). The values are mean±SEM. n=3, *P<0.05. B, Rapamycin treatment normalized the expression of the amino acid responsive genes *Fgf21*, *Gdf15*, *Mthfd2*, *Trib3*, *Asns*, as well as *Gsta1* and the hypertrophy marker, *Myc*. C, *Hif1α* and *Slc7a5* were also normalized with rapamycin treatment, whereas other genes altered by the loss of *Acs1* expression were insensitive to rapamycin. Data are represented by the mean±SEM from 6 biological replicates per condition. The resulting P values from the 2-way ANOVA based on genotype (G), treatment (Tx), and of the interaction (G) are indicated: post-hoc test, *P<0.05, **P<0.01, ***P<0.001, ****P<0.0001 *Acs1*^{flox/flox} vs *Acs1*^{H-/-} within vehicle; †P<0.05, ††P<0.01, †††P<0.001, ††††P<0.0001 vehicle vs rapamycin within genotype. ANOVA indicates analysis of variance; mTOR, mechanistic target of rapamycin; S6K, S6 kinase.

reliance on amino acids for energy initiates this response. Also among the amino acid responsive genes is *Fgf21*, whose gene product secreted by liver, skeletal muscle, pancreas, and

adipose tissue regulates glucose and lipid metabolism during fasting.³⁷ *Fgf21* expression was not increased in liver from *Acs1*^{H-/-} mice (data not shown) suggesting that the

Table 2. Gene Expression Changes in *Acs1*^{H-/-} Hearts

mRNA	Description	Fold Change Microarray	Fold Change qPCR
<i>Srebf1</i>	Sterol regulatory element binding transcription factor 1	2.33	2.91**
<i>Hif1α</i>	Hypoxia inducible factor 1, alpha subunit	2.22	1.63*
<i>Trib3</i>	Tribbles homolog 3	13.10	13.17**
<i>Pdk4</i>	Pyruvate dehydrogenase kinase, isoenzyme 4	5.20	6.10****
<i>Myc</i>	Myelocytomatosis oncogene, transcript variant 1	5.11	6.54**
<i>Gdf15</i>	Growth differentiation factor 15	37.78	76.93****
<i>Fgf21</i>	Fibroblast growth factor 21	30.02	153.17***
<i>Mthfd2</i>	Methylene tetrahydrofolate dehydrogenase	17.79	32.80***
<i>Asns</i>	Asparagine synthetase	4.26	17.49**
<i>Gsta1</i>	Glutathione S-transferase, alpha	20.81	14.65**

The relative fold change in gene expression identified via microarray analysis and subsequently validated via qPCR analysis, *P<0.05, **P<0.01, ***P<0.001, ****P<0.0001.

Table 3. Functional Clustering of Gene Expression Changes in *Acs1*^{H-/-} Hearts

Functional Cluster	Genes	ES	FE
Increased expression in <i>Acs1</i> ^{H-/-}			
Aminoacyl-tRNA synthetases	<i>lars, Cars, Nars, Sars, Aars, Lars, Ubc, Rps2</i>	3.2	8.6
Ribosome	<i>Gm10653, Rpl17, Mrpl27, Ubc, Rpl3, Rpl221l, Mrpl48, Rpl10a, Rps21, Rps2, Cpeb1, Nhp2, Cryab, Thbs4</i>	2.9	3.7
Flavoproteins	<i>Acox1, Aox1, Fdxr, Nqo1, Sardh, Por, Dus2l, Retsat</i>	2.5	4.8
Peroxisome	<i>Acox1, Ech1, Mlycd, Hsd12, Ehhadh, Ephx2, Cat</i>	2.2	5.5
Sarcomere	<i>Ankrd23, Acta1, Cryab, Abra, Myh7, Trim63</i>	2.2	5.0
Regulation of apoptosis	<i>Htatip2, Nol3, Htt, Klf10, Aars, Prdx1, Ddit3, Atf5, Hif1a, Agt, Bcl2, Plcg2, Phlda3, Myc, Ifi204, Angptl4</i>	2.0	2.1
Alanine, aspartate, glutamine, and glutamate metabolism	<i>Glul, Adssl1, Asns, Cad</i>	1.5	8.3
Regulation of fatty acid and lipid metabolism	<i>Srebf1, Mlycd, Agt, Angptl4</i>	1.5	8.8
Decreased expression in <i>Acs1</i> ^{H-/-}			
Transcription regulation	<i>Camta1, Ppara, E2F3, Tshz1, Taf1D, Zfp639, Rest, Zfp768, Cxhc1, Max, Taf5L, Mll5, Myocd, Tsc22D4, Gata6, Tef, Zfp410, Tfcp2, Per1, Hbp1, Zfp687, Rarb, Thap11, Dedd2, Ccar1, Zfp422, Zfp329, Rcor3, Rcor2, Zfp30, Taf8, Gabpa, Hmbox1, Zfx, Mecp2, Zfp672, Creb5, Zfp322A, Mbd1, Zbtb43, Zfp579, Zfp770, Trim33, Ncoa6, Mnt, Pprc1, Phf21A, Mpv17, Zpf612, Mif1, Csdcc2, Pkig, Zpf655, Neo1, Arid2, Meis2, Cenpf, Lass4</i>	5.8	2.0
Zinc finger region	<i>Zfp329, Zfp579, Zfp770, Zfp30, Zfx, Zfp672, Zfp639, Zfp322A, Zfp687, Rest, Zfp768, Zpf422, Tshz1, Zfp410, Zbtb43</i>	4.0	4.3
Membrane-enclosed lumen	<i>Pdp1, Midn, E2F3, Neat1, Bnip3, Rest, Arid2, Zfp768, Cxhc1, Alas1, Mll5, Myocd, Gata6, Fign, Zfml, Ivd, Tfcp2, Hspa5, Top2B, Dedd2, Luc7L3, Ccar1, Rcor2, Taf8, Mphosph10, Cenpf, Mbd1, Zfp655, Ppm1K, Ncoa6, Phf21A</i>	3.9	2.2
Ion binding	<i>Pdp1, Apobec2, Ppara, Agtppbp1, Dicer1, Adcy6, Pdlim3, Zfp639, Rest, Kcnj12, Kcnj11, Mll5, Trim8, Zfml, Gata6, Rarb, Zfp687, 201011101Rik, Kcnq1, Zfp422, Zfp329, Car14, Zfp30, Zfx, Zfp322A, Gmpr, Tecr, Mbd1, Trim35, Prune, Zfp655, Trim33, Ppm1K, Rnf139, Usp20, Zadh2, Pla2G5, Slc39A14, Myl7, Sord, Tshz1, Zfp612, EglN1, Nhlrc1, Arid2, Zfp768, Cxhc1, Acs1, Zfp410, Eno3, Efcab2, Scn5A, Thap11, Mat2A, Ruy1, Zfp672, Creb5, Zbtb43, Ppa2, Mical1, Ick, Zfp579, Dsg2, Zfp770, Zfp207, Mpped2, Sh3Rf2, Phf21A, Abl2, Bmpr1A</i>	2.9	1.4
Zinc finger	<i>Zfp422, Zfp329, Tshz1, Zfp612, Zfp30, Zfx, Zfp672, Creb5, Zfp639, Zfp322A, Rest, Arid2, Zbtb43, Zfp768, Zfp579, Zfp655, Zfp770, Zfml, Zfp207, Zfp410, Zfp687</i>	2.9	2.2
Fibronectin, type III	<i>Epha4, Fn timer, Myom2, Speg, Cmya5, Obsl1, Neo1, Myom1, Insr</i>	2.3	3.4
Negative regulation of transcription	<i>Rcor2, Gabpa, Dicer1, Pkig, Mecp2, Bnip3, Cenpf, Zfp639, Rest, Myocd, Per1, Phf21A, Rarb, Kcnq1, Ednra</i>	1.6	2.1
Regulation of apoptosis	<i>Aifm2, Mecp2, Cenpf, Bnip3, Adora1, Ciapin1, Akt1, Trim35, Mnt, Rarb, Perp, Pik3R1, Dedd2, Ccar1</i>	1.4	1.8
Phosphate metabolic process and phosphorylation	<i>Pdp1, Alpk2, Stk35, Mecp2, Adrbk2, Ptfn21, Adora1, Ppa2, Gak, Akt1, Epha4, Ick, Speg, Dusp27, Ppm1K, Insr, Ipmk, Abl2, Pik3R1, Bmpr1A</i>	1.4	1.6
Striated muscle tissue development	<i>Gata6, Dicer1, Dok7, Pdlim3, EglN1, Rarb</i>	1.3	3.1

Genes that were upregulated or down regulated (Figure 1B) were analyzed for functional clustering using DAVID.^{19,57,58} Each functional cluster is listed with the genes comprising the cluster, as well as the enrichment score (ES), a measure of significance using a modified Fisher Exact,^{19,57,58} and the fold enrichment (FE), which represents the increase in the number of genes present in the differential gene list for a given pathway compared to the expected frequency of genes associated with that pathway in the entire mouse genome.

increase in *Fgf21* expression in the heart was caused by the loss of *Acs11* activity specifically in cardiac tissue. We hypothesized that the upregulation of the amino acid response was secondary to the elevated mTORC1 activity. Indeed, when we treated mice with the mTOR inhibitor rapamycin, we observed a marked attenuation of the induced amino acid responsive genes, including *Fgf21*, *Gdf15*, *Mthfd2*, *Trib3*, *Asns*, and *Gsta1* (Figure 3B) as well as *Hif1 α* and the leucine transporter *Slc7a5* (Figure 3C), confirming that their upregulation was secondary to the elevated mTORC1 activity. Although *Srebp1* is regulated, in part, by mTOR,¹⁴ the increased expression of *Srebp1* did not diminish with rapamycin treatment, nor did the expression of *Acot1* and *Acot2* (Figure 3C), which are cytosolic thioesterases that are upregulated by PPAR α and HNF α .³⁸ Major down-regulated genes that did not respond to rapamycin included: *Pfkfb1*, which encodes the regulating enzyme for gluconeogenesis and glycolysis; *Gpr22*, which encodes an orphan G-protein coupled receptor; and *Sesn1*, which encodes a protein involved in antioxidant defense (Figure 3C). Consistent with the transcriptional signature indicative of heightened cellular stress via increased expression of amino acid responsive genes, and persistent protein synthesis via mTOR activation in *Acs11*^{H^{-/-}} hearts, we also observed an increase in several genes associated with the amino acid deprivation response,³⁹ including activating transcription factor 3 (*Atf3*), cysteinyl-tRNA synthetase (*Cars*), Kruppel-like factor 10 (*Klf10*), chromobox homolog 4 (*Cbx4*), interferon-related developmental regulator 1 (*Ifrd1*), arrestin domain containing 4 (*Aradc4*), and seryl-aminoacyl-tRNA synthetase (*Sars*).

Thus, the global expression analysis of *Acs11*^{H^{-/-}} ventricles confirms the increase in mTORC1 activity and its downstream mRNA regulation, together with expected markers of cardiac hypertrophy. Furthermore, the coordinated increase in amino acid response-related genes, amino acid deprivation genes, and glutathione S-transferase/peroxidase expression (*Gsta1/2*) appears to represent compensatory pathways that are activated in response to the enhanced mTORC1 activity, perhaps to maintain cardiac function by countering the effect of mTOR signaling on protein synthesis and the oxidative stress associated with chronic mTOR activation (see below).

Metabolomic Profiling in *Acs11*^{H^{-/-}} Ventricles Confirmed Increased Glycolysis as Well as Enhanced Cysteine and Glutathione Metabolism

Although much can be inferred from global transcriptional approaches, advances in metabolomics have offered new insights into cellular metabolism through the quantitative analysis of hundreds of metabolites.⁴⁰ We hypothesized that preventing hearts from using FA as an oxidative fuel source

would be likely to reveal numerous glycolytic products, while also providing clues into other pathways altered at the metabolite level. To measure metabolite changes, we used a dual platform consisting of GC- and LC-TOFMS that quantitatively measured 157 and 115 metabolites, respectively, from control and *Acs11*^{H^{-/-}} hearts. Metabolite concentrations were normalized for each platform independently prior to statistical analysis (Figure 4). After merging metabolite concentrations from both platforms into a single dataset, the platform itself was the highest source of variance (data not shown); therefore, we analyzed each platform independently and compared across the 2 genotypes. Similar to the global transcriptional analysis, both PCA and partial least squares (PLS) analysis demonstrated that the predominant source of variance in the metabolite data was genotype, suggesting that substantial differences exist in the metabolite concentrations that are dependent on the genotype of the sample (Figure 5).

We again used a 2-class SAM algorithm to identify individual metabolite concentrations that differed between the 2 groups and identified 47 and 13 species from LC-TOFMS and GC-TOFMS, respectively (FDR<5%, Figure 6A and 6B). The 60 metabolite concentrations and samples were then subjected to unsupervised hierarchical clustering (Figure 6C). As expected, the samples (represented by columns) clustered based on genotype and the metabolites (represented by rows) clustered into 2 primary nodes based on the direction of change. Given the reliance on glucose metabolism in *Acs11*^{H^{-/-}} hearts, we were not surprised to find that several glycolytic metabolites were increased in *Acs11*^{H^{-/-}} hearts. Among the metabolites that had increased the most compared with control hearts were the glycolytic metabolites fructose, fructose 6-phosphate, mannose, mannitol, mannose 6-phosphate, and glucose 6-phosphate; additionally, we found increased levels of metabolites downstream from the pentose phosphate pathway (ribitol) and the TCA cycle (succinate).

To further confirm that glycolysis is indeed increased in *Acs11*^{H^{-/-}} hearts, we measured oxidation of [1-¹⁴C]- and [2-¹⁴C]pyruvate to assess PDH activity and TCA cycle flux, respectively. Despite increased *Pdk4* mRNA expression (Table 2), which is generally regarded as indicating depressed glucose metabolism, PDK4 protein levels did not differ between *Acs11*^{H^{-/-}} mice and their control *Acs11*^{flox/flox} littermates (Figure 7A), whereas GLUT1 levels were significantly higher in *Acs11* knockout mice (Figure 7B), in agreement with the previously observed increase in glucose intake with *Acs11* deficiency.¹⁰ In addition, compared with controls, PDH activity and TCA cycle flux were also higher in *Acs11*^{H^{-/-}} hearts (Figure 7C and 7D), indicating increased use of pyruvate to produce energy and, thus, higher rates of glycolysis in ACSL1-deficient hearts.

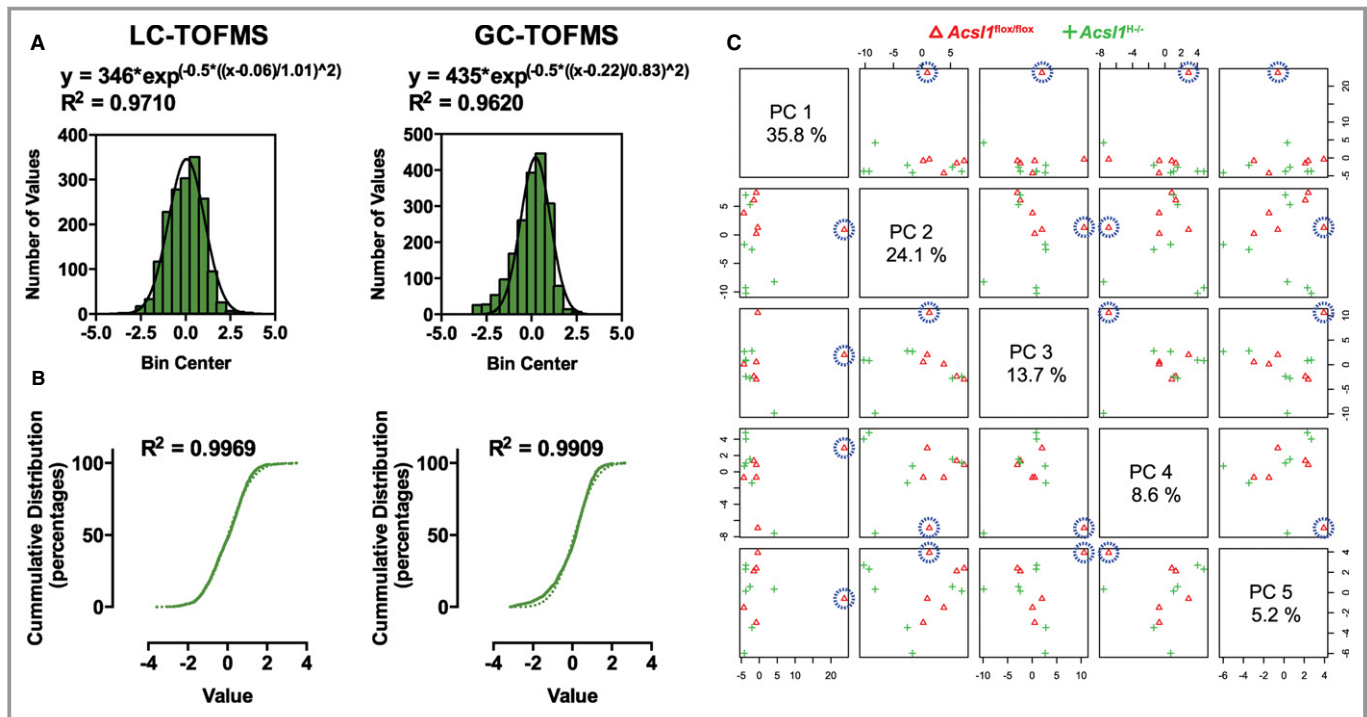


Figure 4. Normalization of metabolite concentrations results in Gaussian distributions. Prior to statistical analysis, the metabolite counts from the LC-TOFMS and GS-TOFMS were log transformed and mean-centered. A, The frequency distributions were plotted with a bin width of 0.5 (green bars) and subsequently fit to a Gaussian distribution curve (solid black line, equation and R^2 value as indicated). B, To remove any potential bin size bias, the same data were analyzed with a cumulative frequency distribution plot. If the data follow a Gaussian distribution, the cumulative distribution has a sigmoidal shape, as shown here (green line). The non-linear fit is also plotted (dotted line) with the corresponding R^2 value provided. C, *Outlier analysis of GC-TOFMS metabolites.* Principal component analysis (PCA) of metabolite concentrations from 13 heart samples measured on the GC-TOFMS platform. There was a single sample that did not cluster with either genotype (highlighted by the blue circle) and contributed to over 35% of the variance as measured via PCA. This sample was removed from the GC-TOFMS statistical analysis. GC- and LC-TOFMS indicates gas chromatography and liquid chromatography-time of flight mass spectrometry.

In addition to the strong glycolytic signals in *Acs1*^{H^{-/-}} hearts, a second dominant class of metabolites was amino acids and intermediates of amino acid metabolism. Amino acids can function as regulatory molecules in increasing mTOR activity and its effects on translation and proteolysis. In particular, sulfur-containing amino acids such as cysteine play important roles in transcriptional regulation, but also in controlling the oxidative balance in tissues. Tissue levels of cysteine are normally maintained to meet the need for both protein and coenzyme A synthesis, as well as for the synthesis of the intracellular antioxidant glutathione. To assess whether glutathione metabolism and oxidative stress were affected by cardiac-specific *Acs1* deficiency, we first analyzed GSK-3 β translocation from the cytosol to mitochondrial membranes in control vs *Acs1*^{H^{-/-}} mice.⁴¹ Compared with their control littermates, *Acs1*^{H^{-/-}} mice showed a 2-fold increase in GSK-3 β in the mitochondrial fraction, suggesting the presence of increased oxidative stress in response to cardiac ACSL1 deficiency (Figure 8A). Despite lower levels of 8-hydroxy-2'-deoxyguanosine in knockout mice, suggesting less DNA damage (Figure 8B), cardiac-specific *Acs1* deficiency resulted

in a higher amount of oxidized glutathione (GSSG), and a 15% lower GSH/GSSG ratio in *Acs1*^{H^{-/-}} mice, further confirming the increase in oxidative stress possibly restricted to glutathione metabolism.

Surprisingly, of the 60 differentially expressed metabolites in *Acs1*^{H^{-/-}} hearts, more than 20% (13 metabolites) mapped to cysteine and glutathione metabolism (Figure 9). Together with the robust increase in both *Gsta1* and *Gsta2* expression (Table 2), the abrogation of *Gsta1* activation with rapamycin (Figure 3B), and the increase in oxidized glutathione and other oxidative stress markers analyzed (Figure 8), these data suggest that a compensatory increase in cysteine and glutathione metabolism may be an essential response to minimize the increased oxidative stress that accompanies glucose-initiated mTOR-activation and the resulting cardiac hypertrophy.

Discussion

ACSL1 comprises 90% of total ACSL activity in the heart and directs activated FA towards mitochondrial β -oxidation. Activated FA normally provide 60% to 90% of

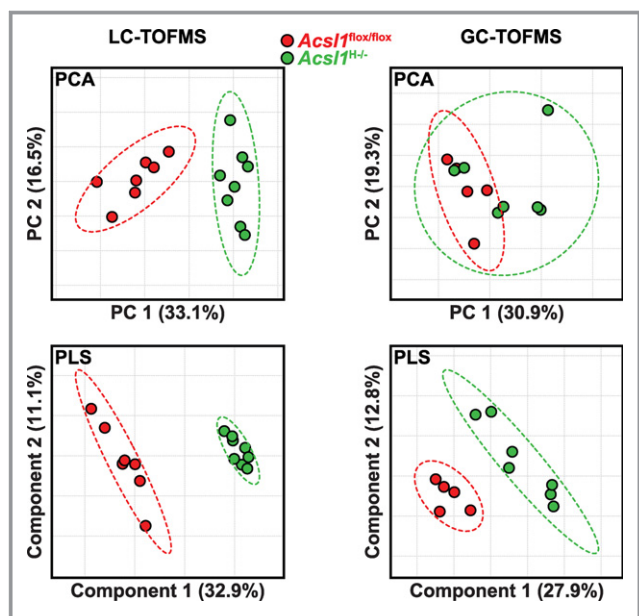


Figure 5. Metabolomic profiling reveals that loss of *Acs1* expression alters the cardiac metabolite profile. Levels of 115 or 157 metabolites measured by either LC-TOFMS (left) or GC-TOFMS (right), respectively, were subjected to both unsupervised (PCA, upper) and supervised (PLS-DA, lower) multivariate data analysis. Data are represented using scatter plots of the first 2 components and confidence ellipses categorized by genotype represent 2 standard deviations. GC- and LC-TOFMS indicates gas chromatography and liquid chromatography-time of flight mass spectrometry; PCA, principal component analysis; PLS-DA, partial least squares discriminant analysis.

the substrate used by the heart for energy, but when ACSL1 is absent, FA oxidation decreases more than 90%.⁹ In compensation, glucose uptake, as indicated by uptake of non-metabolizable 2-deoxy[¹⁴C]glucose, increases 8-fold, suggesting that glucose is the major energy source for the ACSL1-deficient heart.¹⁰ This increase in glucose use results in diminished AMP-activated kinase activity, an 8-fold increase in mTORC1 activity, and mTOR-mediated cardiac hypertrophy.^{9,10}

mTORC1 is a major regulator of cell growth and proliferation and responds to cellular energy levels, stress, and nutrients, particularly amino acids and glucose.⁴² Activation of mTORC1 causes phosphorylation of p70 S6K, which increases protein synthesis, and 4E binding protein, which promotes protein translation.⁴³ mTOR kinase activity is suppressed by the tuberous sclerosis complex 1/2 (TSC1/2). When AMPK is active, it phosphorylates and activates TSC1/2 so that mTOR is inactivated. Although AMPK is usually thought of as reacting to low cellular energy levels, particularly an increased ratio of AMP to ATP, AMPK activity is down-regulated in *Acs1*^{H-/-} hearts, despite normal intracellular concentrations of ATP and AMP.⁹ Down-regulation of AMPK relieves the TSC1/2-mediated suppression of mTORC1 and allows it to be active.

Hemodynamic stress increases carbohydrate use and structural remodeling, both attributable to mTORC1 activation.⁴⁴ Mechanical efficiency is said to be impaired when FA oxidation is high, possibly because the rate of O₂ consumption is higher per amount of ATP generated.^{2,45} In addition, high cytosolic concentrations of FA are potentially subject to a futile ATP-wasting cycle via UCP-3 and thioesterases, with a resulting loss of protons.² Nevertheless in some instances, reliance on glucose may be detrimental to function, given that upregulated mTOR activity promotes hypertrophy and contractile dysfunction in perfused working hearts.⁸ Although the hypertrophy that develops in ACSL1 null hearts is similarly attributable to mTORC1 activation, because it is abrogated by rapamycin treatment, diastolic rather than systolic function is impaired in *Acs1*^{H-/-} hearts.¹⁰

A comprehensive study of gene expression in normal MEFs and in MEFs with activated mTORC1 because of deficient TSC1 or TSC2 showed major changes related to the S6K-mediated hypoxia-inducible transcription factor *Hif1* α and to SREBP1 and SREBP2.¹⁴ These transcriptional targets of mTORC1 were upregulated independent of growth factors and were suppressed by rapamycin; mTORC1-controlled genes included 239 genes that were enriched in pathways of glycolysis, the pentose phosphate shunt, and FA and cholesterol biosynthesis. mRNAs that increased in the MEFs included those encoding *Glut1*, which enhances glucose entry, almost all the glycolytic and pentose phosphate pathway enzymes, and enzymes in the pathways of lipid, FA, and sterol synthesis. The significance of the mRNA upregulation was confirmed by increased substrate flux through the relevant pathways. mTORC1 upregulation of *Hif1* α was responsible for targeting glycolytic genes and for the increased processing of SREBP1 and SREBP2 to active nuclear forms which regulated the pentose phosphate pathway and lipid synthesis genes.¹⁴

To better understand the metabolic changes that occur with substrate switching in heart from FA to glucose, and to determine how these changes were related specifically to chronically activated mTORC1, we used *Acs1*^{H-/-} mice to ask how a fully differentiated tissue would respond to mTORC1 activation and how closely the changes would correspond to the alterations found in MEFs with increased mTORC1.¹⁴ We examined gene arrays and tested whether the increases observed in a subset of upregulated genes would be diminished when mTOR was inhibited by rapamycin treatment. In addition, we used unbiased metabolomics to identify changes in cardiac metabolic pathways that occurred when reliance on glucose for energy was essential. Similar to the data with activated mTORC1 in MEFs, the gene array obtained from *Acs1*^{H-/-} hearts showed upregulated *Hif1* α , *Srebp1* (*Srebf1*), and several glycolytic genes (eg, *Pfkfb1*). However, in *Acs1*^{H-/-} hearts, genes involved in the pentose shunt and in FA and sterol synthesis were not altered. Instead, we noted

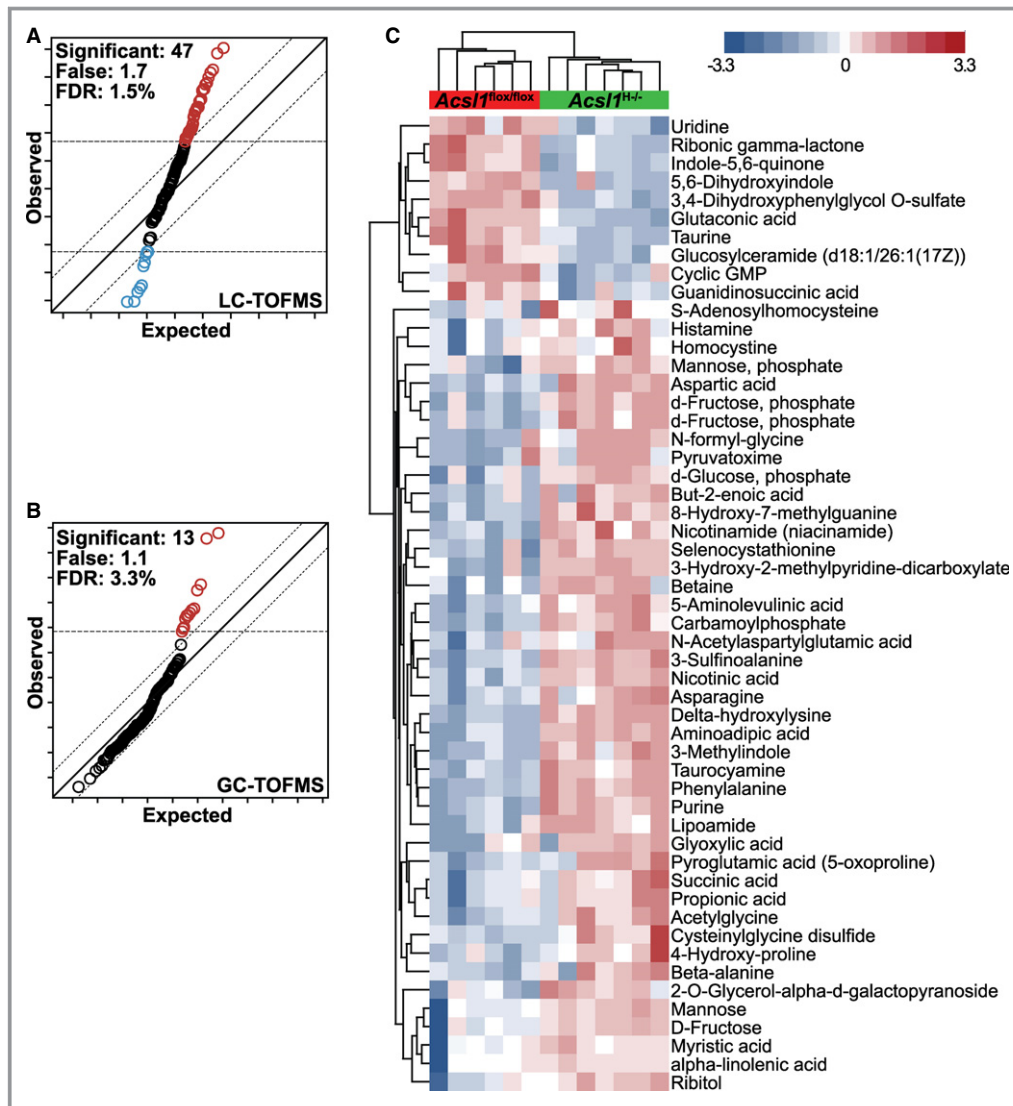


Figure 6. Differential metabolite analysis in *Acs1*-deficient hearts. A and B, Significance analysis of metabolites (SAMet) plot of observed scores plotted against the expected scores in heart extracts from either control or *Acs1*^{H^{-/-}} mice obtained from the LC-TOFMS (A) or GS-TOFMS (B). The solid line represents observed=expected, whereas the hashed lines indicate the significance threshold based on $\Delta=1.2$. The metabolites identified as significantly different are indicated by red and blue open circles, indicating higher and lower concentrations, respectively, of these genes in *Acs1*^{H^{-/-}} relative to control mouse hearts. The number of differential metabolite concentrations, the number of predicted false positives, and the false discovery rate (FDR) are provided. C, Unsupervised hierarchical clustering of the combined LC- GC-TOFMS data set using the differential metabolites identified by SAMet in *Acs1*^{H^{-/-}} and control mouse hearts. GC-TOFMS indicates gas chromatography-time of flight mass spectrometry.

striking upregulation of additional mTOR-dependent pathways, particularly the amino acid responsive genes, peroxisomal genes, and genes involved in the regulation of apoptosis and cell stress. Several of these genes have been previously identified as targets of mTORC1: *Fgf21* and *Gdf15* are prominent in CCK-mediated pancreatic growth⁴⁶ and *Gdf15* in ovarian cancer.⁴⁷ Our study of *Acs1*^{H^{-/-}} hearts also showed diminished expression of numerous genes related to transcriptional regulation and zinc finger factors.

Cardiac stresses like hypertension alter predominant substrate use from FA to glucose.² mTORC1 is now seen as a major cause of cardiac hypertrophy, as it both stimulates cell growth and inhibits autophagy.⁴⁸ mTORC1 activation underlies the hypertrophy that occurs in hypertensive SHR rats⁴⁹ and in *Acs1*^{H^{-/-}} mice that cannot use FA for energy. Our study in mice is consistent with data from working hearts showing that perfusion with glucose causes metabolic changes that precede cardiac structural remodeling. In both

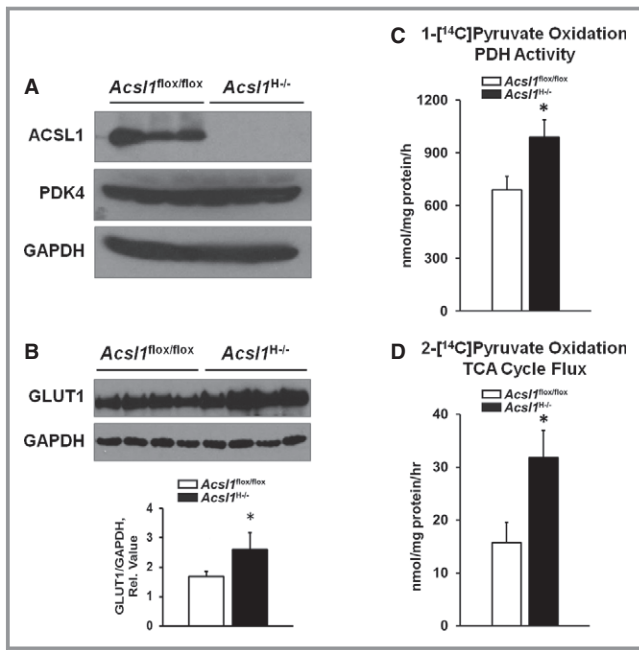


Figure 7. Cardiac-specific *Acs1* deficiency leads to increased glucose metabolism. A and B, Representative immunoblots against PDK4, deglycosylated GLUT1 and GAPDH (loading control) from ventricles of male control and *Acs1*^{H^{-/-}} mice 10 weeks after tamoxifen treatment. The ratio of GLUT1 to GAPDH is shown (B, bottom). The values are mean±SEM. n=3 to 4, **P*<0.05. C and D, [¹⁻¹⁴C]- and [²⁻¹⁴C]pyruvate oxidation to CO₂ from control and *Acs1*^{H^{-/-}} ventricular homogenates 10 weeks after tamoxifen injection. The values are mean±SEM. n=5 to 6, **P*<0.05. TCA indicates tricarboxylic acid.

Acs1^{H^{-/-}} mice⁹ and in isolated rat hearts using glucose and subjected to an elevated workload,⁸ activated AMPK decreases, thereby diminishing phosphorylation of TSC1 and relieving its inhibition of mTORC1; the resulting increase in mTORC1 activity induces cardiac hypertrophy.¹⁰

Metabolomics analysis has not been extensively used to gain information about energy pathways in the heart. In humans with ischemia, increased circulating metabolites include metabolites related to pyrimidine metabolism, and the tricarboxylic acid and pentose phosphate pathways.⁵⁰ A metabolomic analysis of ventricles from cardiomyopathic hamsters showed a mild reduction in glutathione and increased oxidative stress.⁵¹ In our study, the upregulation of 13 metabolites related to cysteine and glutathione metabolism was unanticipated. Perfusion of working rat hearts with glucose causes oxidative stress,⁸ and it is likely that the altered metabolite and gene expression in *Acs1*^{H^{-/-}} hearts, as well as increased oxidized glutathione and other oxidative stress markers analyzed, indicate a response to oxidative stress initiated by either mTORC1 or another aspect of the switch in substrate use. The expression of *Gsta1* and *Gsta2* was 15-fold higher in *Acs1*^{H^{-/-}} hearts than controls,

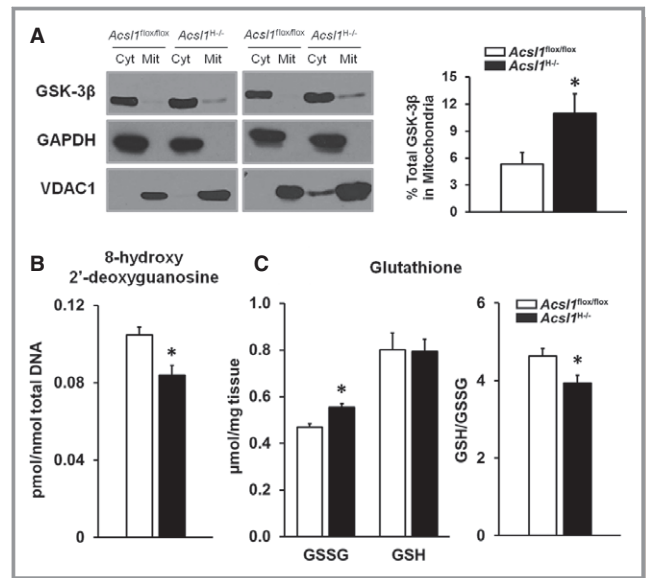


Figure 8. Loss of *Acs1* results in elevated oxidative stress markers in the heart. A, Representative immunoblots against GSK-3β, VDAC1 (mitochondrial marker) and GAPDH (cytosolic marker) from ventricles of male control and *Acs1*^{H^{-/-}} mice 10 weeks after tamoxifen treatment. The levels of GSK-3β and VDAC1 were quantified with ImageJ software, the ratio of GSK-3β to VDAC1 calculated and the percentage of GSK-3β in the mitochondrial fraction of control and *Acs1*^{H^{-/-}} mice is shown (right). The values are mean±SEM. n=4, **P*<0.05. B, 8-hydroxy-2'-deoxyguanosine levels were measured as indication of DNA and RNA damage in left ventricles of male control and *Acs1*^{H^{-/-}} mice 10 weeks after tamoxifen treatment. C, Oxidized (GSSG) and reduced (GSH) levels of glutathione were measured using a colorimetric kit. The values are mean±SEM. n=5 to 6, **P*<0.05.

and rapamycin diminished *Gsta1* expression dramatically, consistent with other studies demonstrating induction of *Gsta1* expression in hearts overexpressing GLUT1⁵² and with induction of *Gsta2* expression by mTOR when cells are stimulated by insulin^{53,54} or by cytoprotective agents.⁵⁵

When glucose flux into the heart was enhanced by cardiac-specific overexpression of the glucose transporter GLUT1, PPARα expression and FA oxidation were diminished, oxidative stress increased, and mild contractile dysfunction occurred.³² Similarly, when isolated hearts were perfused with glucose and subjected to a high workload, mTOR was activated and ER stress and defective contractile function were induced; the ER stress and contractile defects were abrogated by pretreatment with rapamycin, demonstrating the specific role of mTOR in the manifestation of these cardiac phenotypes.⁸ Studies using 2-deoxyglucose, which can be converted to 2-deoxyglucose-6-phosphate but cannot be further metabolized, demonstrated that conversion of glucose to its phosphorylated product is required for mTOR activation.⁵⁶ Thus, the authors concluded that dependence on glucose use causes metabolic changes that activate mTOR to regulate heart remodeling.⁸ Our study in

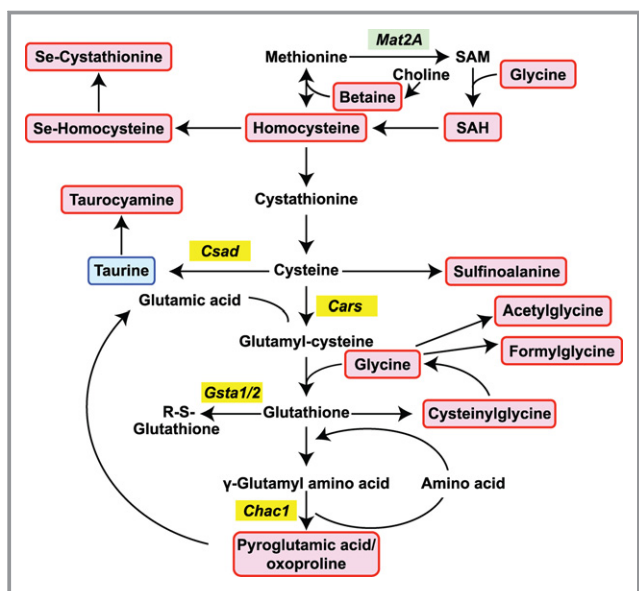


Figure 9. *Acs1*-dependent changes in metabolites in the biochemical pathway involving cysteine and glutathione metabolism. Metabolite concentrations are identified as either increased (red) or decreased (blue) in *Acs1*^{H^{-/-} hearts relative to control hearts. Upregulated (yellow) and downregulated (green) genes in this pathway are also shown (see Table S1).}

living mice whose cardiac demand for glucose oxidation is dramatically enhanced supports this interpretation. In addition, we show that a deficit in the use of FA for energy causes numerous major changes in gene expression, many of which, but not all, can be attributed to mTORC1 activation. Although substrate switching from FA to glucose did not affect cardiac systolic function in *Acs1*^{H^{-/-} hearts, diastolic function was impaired.¹⁰ Thus, the potential for harm related to oxidative stress and aberrant physiology suggests that a switch from the use of FA to glucose may not be entirely benign.}

Sources of Funding

This work was supported by NIH grants DK59935 (Coleman), HL104129 (Willis), 5R37HL065619 (Patterson), 5R01GM-061728 (Patterson), and the University of North Carolina Nutrition Obesity Research Center DK056350, the Fondation Leducq Transatlantic Network of Excellence (Patterson, Willis), NIH Predoctoral Training grants T32HL069768 (Ellis) and T32HL069768 (Grevengoed), and pre-doctoral fellowships 0815054E (Ellis) and 13PRE16910109 (Grevengoed) and 12GRNT12030144 (Coleman) from the American Heart Association Mid-Atlantic Division.

Disclosures

None.

References

- van der Vusse GJ, Glatz JF, Stam HC, Reneman RS. Fatty acid homeostasis in the normoxic and ischemic heart. *Physiol Rev.* 1992;72:881–940.
- Stanley WC, Recchia FA, Lopaschuk GD. Myocardial substrate metabolism in the normal and failing heart. *Physiol Rev.* 2005;85:1093–1129.
- Ventura-Clapier R, Garnier A, Veksler V. Energy metabolism in heart failure. *J Physiol.* 2004;555:1–13.
- Izzo P. Metabolic toxicity of the heart: insights from molecular imaging. *Nutr Metab Cardiovasc Dis.* 2010;20:147–156.
- Liao R, Jain M, Cui L, D'Agostino J, Aiello F, Luptak I, Ngoy S, Mortensen RM, Tian R. Cardiac-specific overexpression of GLUT1 prevents the development of heart failure attributable to pressure overload in mice. *Circulation.* 2002;106:2125–2131.
- Luptak I, Yan J, Cui L, Jain M, Liao R, Tian R. Long-term effects of increased glucose entry on mouse hearts during normal aging and ischemic stress. *Circulation.* 2007;116:901–909.
- Luptak I, Balschi JA, Xing Y, Leone TC, Kelly DP, Tian R. Decreased contractile and metabolic reserve in peroxisome proliferator-activated receptor- α -null hearts can be rescued by increasing glucose transport and utilization. *Circulation.* 2005;112:2339–2346.
- Sen S, Kundu BK, Wu HC, Hashmi SS, Guthrie P, Locke LW, Roy RJ, Matherne GP, Berr SS, Terwelp M, Scott B, Carranza S, Frazier OH, Glover DK, Dillmann WH, Gambello MJ, Entman ML, Taegtmeier H. Glucose regulation of load-induced mTOR signaling and ER stress in mammalian heart. *J Am Heart Assoc.* 2013;2:e004796.
- Ellis JM, Mentock SM, Depettillo MA, Koves TR, Sen S, Watkins SM, Muoio DM, Cline GW, Taegtmeier H, Shulman GI, Willis MS, Coleman RA. Mouse cardiac acyl coenzyme a synthetase 1 deficiency impairs Fatty Acid oxidation and induces cardiac hypertrophy. *Mol Cell Biol.* 2011;31:1252–1262.
- Paul DS, Grevengoed TJ, Pascual F, Ellis JM, Willis MS, Coleman RA. Deficiency of cardiac acyl-CoA synthetase-1 induces diastolic dysfunction, but pathologic hypertrophy is reversed by rapamycin. *Biochim Biophys Acta.* 2014;184:1:880–887.
- Chiu HC, Kovacs A, Ford DA, Hsu FF, Garcia R, Herrero P, Saffitz JE, Schaffer JE. A novel mouse model of lipotoxic cardiomyopathy. *J Clin Invest.* 2001;107:813–822.
- Zoncu R, Efeyan A, Sabatini DM. mTOR: from growth signal integration to cancer, diabetes and ageing. *Nat Rev Mol Cell Biol.* 2011;12:21–35.
- Laplante M, Sabatini DM. Mtor signaling in growth control and disease. *Cell.* 2012;149:274–293.
- Duvel K, Yecies JL, Menon S, Raman P, Lipovsky AI, Souza AL, Triantafellow E, Ma Q, Gorski R, Cleaver S, Vander HM, MacKeigan JP, Finan PM, Clish CB, Murphy LO, Manning BD. Activation of a metabolic gene regulatory network downstream of mtor complex 1. *Mol Cell.* 2010;39:171–183.
- Li LO, Ellis JM, Paich HA, Wang S, Gong N, Altshuler G, Thresher RJ, Koves TR, Watkins SM, Muoio DM, Cline GW, Shulman GI, Coleman RA. Liver-specific loss of long chain acyl-CoA synthetase-1 decreases triacylglycerol synthesis and beta-oxidation and alters phospholipid fatty acid composition. *J Biol Chem.* 2009;284:27816–27826.
- Zhao Y, Wieman HL, Jacobs SR, Rathmell JC. Mechanisms and methods in glucose metabolism and cell death. *Methods Enzymol.* 2008;442:439–457.
- He XR, Zhang C, Patterson C. Universal mouse reference RNA derived from neonatal mice. *Biotechniques.* 2004;37:464–468.
- Tusher VG, Tibshirani R, Chu G. Significance analysis of microarrays applied to the ionizing radiation response. *Proc Natl Acad Sci USA.* 2001;98:5116–5121.
- da Huang W, Sherman BT, Lempicki RA. Systematic and integrative analysis of large gene lists using DAVID bioinformatics resources. *Nat Protoc.* 2009;4:44–57.
- Pan L, Qiu Y, Chen T, Lin J, Chi Y, Su M, Zhao A, Jia W. An optimized procedure for metabolomic analysis of rat liver tissue using gas chromatography/time-of-flight mass spectrometry. *J Pharm Biomed Anal.* 2010;52:589–596.
- Fordahl S, Cooney P, Qiu Y, Xie G, Jia W, Erikson KM. Waterborne manganese exposure alters plasma, brain, and liver metabolites accompanied by changes in stereotypic behaviors. *Neurotoxicol Teratol.* 2012;34:27–36.
- Chen T, Xie G, Wang X, Fan J, Qiu Y, Zheng X, Qi X, Cao Y, Su M, Wang X, Xu LX, Yen Y, Liu P, Jia W. Serum and urine metabolite profiling reveals potential biomarkers of human hepatocellular carcinoma. *Mol Cell Proteomics.* 2011;10: M110.004945.
- Xie G, Zhong W, Zheng X, Li Q, Qiu Y, Li H, Chen H, Zhou Z, Jia W. Chronic ethanol consumption alters mammalian gastrointestinal content metabolites. *J Proteome Res.* 2013;12:3297–3306.
- Xia J, Mandal R, Sinelnikov IV, Broadhurst D, Wishart DS. Metaboanalyst 2.0—a comprehensive server for metabolomic data analysis. *Nucleic Acids Res.* 2012;40:W127–W133.

25. Xia J, Psychogios N, Young N, Wishart DS. Metaboanalyst: a web server for metabolomic data analysis and interpretation. *Nucleic Acids Res.* 2009;37:W652–W660.
26. Xia J, Wishart DS. Web-based inference of biological patterns, functions and pathways from metabolomic data using metaboanalyst. *Nat Protoc.* 2011;6:743–760.
27. Liu J, Zhang W, Chuang GC, Hill HS, Tian L, Fu Y, Moellering DR, Garvey WT. Role of TRIB3 in regulation of insulin sensitivity and nutrient metabolism during short-term fasting and nutrient excess. *Am J Physiol Endocrinol Metab.* 2012;303:E908–E916.
28. Lee JH, Kim EJ, Kim DK, Lee JM, Park SB, Lee IK, Harris RA, Lee MO, Choi HS. Hypoxia induces PDK4 gene expression through induction of the orphan nuclear receptor errgamma. *PLoS One.* 2012;7:e46324.
29. Eivers SS, McGivney BA, Fonseca RG, MacHugh DE, Menson K, Park SD, Rivero JL, Taylor CT, Katz LM, Hill EW. Alterations in oxidative gene expression in equine skeletal muscle following exercise and training. *Physiol Genomics.* 2010;40:83–93.
30. Ago T, Sadoshima J. GDF15, a cardioprotective TGF-beta superfamily protein. *Circ Res.* 2006;98:294–297.
31. Kolwicz SC Jr, Tian R. Metabolic therapy at the crossroad: how to optimize myocardial substrate utilization? *Trends Cardiovasc Med.* 2009;19:201–207.
32. Yan J, Young ME, Cui L, Lopaschuk GD, Liao R, Tian R. Increased glucose uptake and oxidation in mouse hearts prevent high fatty acid oxidation but cause cardiac dysfunction in diet-induced obesity. *Circulation.* 2009;119:2818–2828.
33. Stevenson EJ, Koncarevic A, Giresi PG, Jackman RW, Kandarian SC. Transcriptional profile of a myotube starvation model of atrophy. *J Appl Physiol.* 2005;98:1396–1406.
34. Tyynismaa H, Carroll CJ, Raimundo N, Ahola-Erkkila S, Wenz T, Ruhanen H, Guse K, Hemminki A, Peltola-Mjosund KE, Tulkki V, Oresic M, Moraes CT, Pietilainen K, Hovatta I, Suomalainen A. Mitochondrial myopathy induces a starvation-like response. *Hum Mol Genet.* 2010;19:3948–3958.
35. Yatsuga S, Suomalainen A. Effect of bezafibrate treatment on late-onset mitochondrial myopathy in mice. *Hum Mol Genet.* 2012;21:526–535.
36. Fujita Y, Ito M, Nozawa Y, Yoneda M, Oshida Y, Tanaka M. Chop (C/EBP homologous protein) and ASNS (asparagine synthetase) induction in cybrid cells harboring MELAS and NARP mitochondrial DNA mutations. *Mitochondrion.* 2007;7:80–88.
37. Potthoff MJ, Kliewer SA, Mangelsdorf DJ. Endocrine fibroblast growth factors 15/19 and 21: from feast to famine. *Genes Dev.* 2012;26:312–324.
38. Dongol B, Shah Y, Kim I, Gonzalez FJ, Hunt MC. The acyl-CoA thioesterase i is regulated by PPARalpha and HNF4alpha via a distal response element in the promoter. *J Lipid Res.* 2007;48:1781–1791.
39. Sikalidis AK, Lee JJ, Stipanuk MH. Gene expression and integrated stress response in HepG2/C3A cells cultured in amino acid deficient medium. *Amino Acids.* 2011;41:159–171.
40. Heather LC, Wang X, West JA, Griffin JL. A practical guide to metabolomic profiling as a discovery tool for human heart disease. *J Mol Cell Cardiol.* 2013;55:2–11.
41. Tanno M, Kuno A, Ishikawa S, Miki T, Kouzu H, Yano T, Murase H, Tobisawa T, Ogasawara M, Horio Y, Miura T. Translocation of glycogen synthase kinase-3beta (GSK-3beta), a trigger of permeability transition, is kinase activity-dependent and mediated by interaction with voltage-dependent anion channel 2 (VDAC2). *J Biol Chem.* 2014;289:29285–29296.
42. Jewell JL, Guan KL. Nutrient signaling to mTOR and cell growth. *Trends Biochem Sci.* 2013;38:233–242.
43. Howell JJ, Ricoult SJ, Ben-Sahra I, Manning BD. A growing role for mTOR in promoting anabolic metabolism. *Biochem Soc Trans.* 2013;41:906–912.
44. Goodwin GW, Taylor CS, Taegtmeier H. Regulation of energy metabolism of the heart during acute increase in heart work. *J Biol Chem.* 1998;273:29530–29539.
45. Stanley WC, Chandler MP. Energy metabolism in the normal and failing heart: potential for therapeutic interventions. *Heart Fail Rev.* 2002;7:115–130.
46. Gurda GT, Wang JY, Guo L, Ernst SA, Williams JA. Profiling CCK-mediated pancreatic growth: the dynamic genetic program and the role of STATs as potential regulators. *Physiol Genomics.* 2012;44:14–24.
47. Griner SE, Joshi JP, Nahta R. Growth differentiation factor 15 stimulates rapamycin-sensitive ovarian cancer cell growth and invasion. *Biochem Pharmacol.* 2013;85:46–58.
48. Kurdi M, Booz GW. Three 4-letter words of hypertension-related cardiac hypertrophy: TRPC, mTOR, and HDAC. *J Mol Cell Cardiol.* 2011;50:964–971.
49. Soesanto W, Lin HY, Hu E, Lefler S, Litwin SE, Sena S, Abel ED, Symons JD, Jalili T. Mammalian target of rapamycin is a critical regulator of cardiac hypertrophy in spontaneously hypertensive rats. *Hypertension.* 2009;54:1321–1327.
50. Lewis GD, Wei R, Liu E, Yang E, Shi X, Martinovic M, Farrell L, Asnani A, Cyrille M, Ramanathan A, Shaham O, Berriz G, Lowry PA, Palacios IF, Tasan M, Roth FP, Min J, Baumgartner C, Keshishian H, Addona T, Mootha VK, Rosenzweig A, Carr SA, Fifer MA, Sabatine MS, Gerszten RE. Metabolite profiling of blood from individuals undergoing planned myocardial infarction reveals early markers of myocardial injury. *J Clin Invest.* 2008;118:3503–3512.
51. Maekawa K, Hirayama A, Iwata Y, Tajima Y, Nishimaki-Mogami T, Sugawara S, Ueno N, Abe H, Ishikawa M, Murayama M, Matsuzawa Y, Nakanishi H, Ikeda K, Arita M, Taguchi R, Minamino N, Wakabayashi S, Soga T, Saito Y. Global metabolomic analysis of heart tissue in a hamster model for dilated cardiomyopathy. *J Mol Cell Cardiol.* 2013;59:76–85.
52. Pereira RO, Wende AR, Olsen C, Soto J, Rawlings T, Zhu Y, Anderson SM, Abel ED. Inducible overexpression of GLUT1 prevents mitochondrial dysfunction and attenuates structural remodeling in pressure overload but does not prevent left ventricular dysfunction. *J Am Heart Assoc.* 2013;2:e000301.
53. Kang KW, Cho IJ, Lee CH, Kim SG. Essential role of phosphatidylinositol 3-kinase-dependent CCAAT/enhancer binding protein beta activation in the induction of glutathione S-transferase by oltipraz. *J Natl Cancer Inst.* 2003;95:53–66.
54. Langston W, Circu ML, Aw TY. Insulin stimulation of gamma-glutamylcysteine ligase catalytic subunit expression increases endothelial GSH during oxidative stress: influence of low glucose. *Free Radic Biol Med.* 2008;45:1591–1599.
55. Kim SG, Lee SJ. Pi3k, RSK, and mTOR signal networks for the GST gene regulation. *Toxicol Sci.* 2007;96:206–213.
56. Sharma S, Guthrie PH, Chan SS, Haq S, Taegtmeier H. Glucose phosphorylation is required for insulin-dependent mTOR signalling in the heart. *Cardiovasc Res.* 2007;76:71–80.
57. da Huang W, Sherman BT, Lempicki RA. Bioinformatics enrichment tools: paths toward the comprehensive functional analysis of large gene lists. *Nucleic Acids Res.* 2009;37:1–13.
58. da Huang W, Sherman BT, Tan Q, Collins JR, Alvord WG, Roayaei J, Stephens R, Baseler MW, Lane HC, Lempicki RA. The DAVID gene functional classification tool: a novel biological module-centric algorithm to functionally analyze large gene lists. *Genome Biol.* 2007;8:R183.